Computational models for large amplitude nonlinear vibrations of electrostatically actuated carbon nanotube-based mass sensors

Saoussen Souayeh, Najib Kacem

Computational models for large amplitude nonlinear vibrations of electrostatically actuated carbon nanotube-based mass sensors

S. Souayeh, N. Kacem*

FEMTO-ST Institute – UMR 6174, CNRS-UFC-ENSMM-UTBM, 24, chemin de l'Épitaphe, F-25000 Besançon, France

A comprehensive multiphysics model of a cantilevered carbon nanotube (CNT) including geometric and electrostatic nonlinearities is developed. The continuous model is reduced to a finite degree of freedom system by the Galerkin discretization and solved using the harmonic balance method (HBM) coupled with the asymptotic numerical method (ANM). The influence of higher modes on the nonlinear dynamics of the considered resonator is investigated in order to retain the number of modes which will be used by the HBM+ANM procedure. Several simulations are performed for a specific CNT design in order to obtain a wide range of frequency shifts with respect to the mass and position of an added particle. This model is an intuitive way for designers to develop resonant nanosensors vibrating at large amplitudes for mass detection. Particularly, it is demonstrated that the mass and position of a particle can be determined based on the proposed model reduced to the first bending mode coupled with the analytical expressions of the linear frequency shifts for the second and third modes.

1. Introduction

Electromechanical resonators play an important role in a variety of fields [1]. One of the most important applications is the mass detection, particularly, the detection of tiny amounts of mass [2–6]. For highly sensitive tasks, we talk about mass spectrometry. For example, mass spectrometry can provide quantitative identification of individual protein species in real time [7]. Among the most sensitive ones are sensors based on thin film [8], micron-sized cantilevers [9], the acoustic vibratory modes of crystals [10], nanocantilevers [11] and carbon nanotubes [7,12,13]. Mass spectrometers are composed by three parts: analyte ionization, analyte separation and detection [14]. These systems are widely used for several applications such as proteomics [15,16].

The micro [17]/nano [2]-electromechanical systems have large quality factors and reduced dimensions allowing to achieve femtogram ($1fg = 10^{-15}$ g) [3,18], attogram ($1ag = 10^{-18}$ g)[11] and zeptogram [5] ($1zg = 10^{-21}$ g) resolutions. Recently, some devices can reach the mass sensitivity of the range of Dalton ($1\,Da = 1$ AMU) [19–22]. The sensitivity of a resonant mass sensor may be established by two properties: the resonant's effective vibratory mass determined by its geometry and material properties and the stability of the frequency for long and short term governed by intrinsic and extrinsic processes [19].

Nonlinear dynamics is one of the most important properties for NEMS, allowing them to display interesting behaviors. Nonlinearities in nanoresonators can be inertial, geometric [23] or obtained by external forces [24]. A multitude of nonlinear phenomena have been observed in NEMS such as periodic attractors [25], bifurcation topology [26] and bistability [27].

Different methods have been used in order to solve the resulting non-linear equations of motion of a resonator such as the shooting method [28], time integration method [29], perturbation methods [30] and the method of non-linear normal forms [31]. In order to study the vibrational behavior of NEMS, some researches have been done using finite element-formulation [32]. For nonlinear vibrations, it is often required to calculate the periodic solutions of nonlinear differential equations. To this end, numerical methods are used. They are subdivided into two approaches: those relying on the time-domain formulation and those relying on the frequency-domain formulation. The first approach consists on transforming the original differential system into a set of algebraic equations by using an integration algorithm, and then, solving the obtained equations by continuation. The shooting method is an example of this category. The second approach is the harmonic balance method (HBM) for which the unknown variables are decomposed into truncated Fourier series. The choice between the time-domain or the frequency-domain approach depends on whether the periodic solution can be decomposed with a few Fourier components.

Cantilevered sensors are very useful for biological, chemical and physical sensors [3,33,34]. It is commonly known that the dynamic range (DR) of cantilevers is very large compared to the DR of the clamped–clamped beams (>20 times) [35]. Furthermore, the

* Corresponding author. Tel.: +33 381 66 67 02; fax: +33 381 66 67 00.
E-mail addresses: najib.kacem@femto-st.fr, najib.kacem@univ-fcomte.fr (N. Kacem).

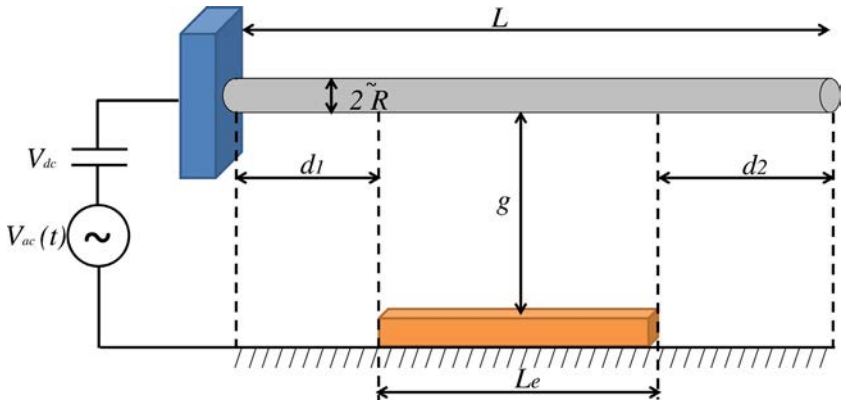

Fig. 1. Schematic of a cantilevered carbon nanotube oscillator electrostatically actuated.

miniaturization of such devices will produce nanocantilevers with higher frequencies [36] and low power consumption, which make them the most appropriate candidates for mass sensing applications.

An attached mass to a cantilever will cause the frequency shift in the fundamental mode of vibration [19,20]. The position and the mass of an added particle will change the mass response of the resonator [37]. Therefore, it is essential to provide a method allowing the simultaneous detection of the mass and position. Such method can be of a great interest for hollow cantilevers [38] in which the molecules are adsorbed on the internal surface at an unknown position. The most sensitive hollow device is the carbon nanotube, since the carbon is a material of choice for ultrasensitive resonators [39–41]. Due to the low mass of the nanotube (few attograms), a tiny amount of atoms deposited onto it represents a significant fraction of the total mass. In addition, nanotubes are mechanically ultra-rigid permitting the increase of the resonance frequency. Two major possibilities of the position of the added molecules on the resonators can be considered: the particules are added as a point mass [42] or are in a homogeneous layer covering all of the cantilever [5]. The response of the cantilever is sensitive to the variation of the position of the mass [43]. So, the particle position should be known in order to determine effectively the mass value. Several investigations were done in order to develop a technique allowing the simultaneous position and mass detection. But, such algorithms are very complicated and demand a sophisticated mathematical methods to be solved. The alternative to avoid this problem is to find relations between mass and position of the added particules and the resonant frequencies of the cantilever [44] by measuring the resonant frequencies of the beam without and with added mass for several vibrational modes.

In this paper, the nonlinear dynamics of a carbon nanotube (CNT) is investigated. To this end, a multiphysics model including the main sources of nonlinearities is developed. The mechanical nonlinearity is principally geometric while the electrostatic one is expanded in Taylor series up to the fifth order to take into account all relevant nonlinear terms for NEMS [26,45]. In order to investigate the responses of a CNT oscillator for the detection of the mass and the position of an added particle, an efficient numerical procedure has been used. The main idea is to provide numerical tools for NEMS designers in order to enhance the performances of resonant mass sensors.

Firstly, a design of an electrostatically actuated CNT is proposed and modeled. The electrode has the particularity to be placed at a specific position relatively to the nanotube in order to enlarge the NEMS dynamic range and localize a specific position of the transduction close to the fixed end of the CNT. Then, the Galerkin discretization procedure is used in order to transform the multiphysics continuum problem into a finite system of nonlinear ordinary differential equations in time. The reduced-order model is solved numerically using the harmonic balance method coupled with the asymptotic numerical continuation technique. Based on these numerical methods, the frequency responses of the CNT for several design parameters are derived and investigated in the linear and nonlinear configurations, so that, we can retain the number of modes which gives the most accurate results.

Finally, the frequency shifts of the resonance peaks are numerically tracked on three modes for a particular CNT design and several added masses in different positions along the NEMS length. The maps of the frequency shifts are derived with respect to the mass and position of the added particle for linear and nonlinear configurations. By comparing the two cases, a hybrid analytical–numerical approach is proposed which is computationally less time consuming allowing the construction of larger frequency shift maps in order to enhance the mass detection accuracy.

2. Design and model

We consider a carbon nanotube (CNT) resonator depicted in Fig. 1. It consists of a single nanocantilever with an annular cross section initially straight, clamped at one end and free at the other end. It is actuated by an electrostatic force $v(\tilde{t}) = V_{dc} + V_{ac}\cos(\tilde{\Omega}\tilde{t})$, where V_{dc} is the *dc* polarization voltage, V_{ac} is the amplitude of the applied *ac* voltage, $\tilde{t}$ is the time and $\tilde{\Omega}$ is the excitation frequency. The electrode is positioned at a distance d_1 from the fixed end in order to place a piezoelectric or piezoresistive transduction [46] and at a distance d_2 from the free extremity in order to enlarge the oscillator dynamic range below the upper bound limit which is the pull-in [28], since the coefficients of the bending modes are lower at $L - d_2$ in comparison with the ones at L.

The CNT is modeled as an Euler-Bernoulli beam of length L and with a quality factor Q. It has an internal radius $\tilde{R_1}$, an external one $\tilde{R_2}$.

2.1. Equation of motion

The equation of motion of the CNT can be written as [13]:

$$EI\partial_{\tilde{x},\tilde{x},\tilde{x},\tilde{x}}\tilde{w} + \rho A\partial_{\tilde{t},\tilde{t}}\tilde{w} + \tilde{c}\partial_{\tilde{t}}\tilde{w} = EI\partial_{\tilde{x}}(\partial_{\tilde{x}}\tilde{w}\partial_{\tilde{x}}(\partial_{\tilde{x}}\tilde{w}\partial_{\tilde{x},\tilde{x}}\tilde{w})) + \mathcal{H}(\tilde{x})\tilde{F} \quad (1)$$

$$\mathcal{H}(\tilde{x}) = H(\tilde{x} - d_1) - H(\tilde{x} - L + d_2)$$

where $\partial_{\tilde{x}}$ denotes the partial differentiation with respect to $\tilde{x}$ which is the coordinate along the nanotube length L, $\partial_{\tilde{t}}$ is the partial differentiation with respect to the time $\tilde{t}$, $\tilde{w}(\tilde{x},\tilde{t})$ is the in-plane bending deflection, E is the effective Young's modulus, $I = (\pi/4)(\tilde{R_2}^4 - \tilde{R_1}^4)$ is the moment of inertia of the circular cross-section, ρ is the density of the nanotube material, $A = \pi(\tilde{R_2}^2 - \tilde{R_1}^2)$

is the cross-section area and $\tilde{c}$ is the coefficient of the viscous damping per unit length.

The carbon nanotube is subject to the electrostatic actuation $\mathcal{H}(\tilde{x})\tilde{F}$, where $\mathcal{H}(\tilde{x})$ includes heaviside functions H in order to indicate the position of the electrode with respect to the oscillator, wherein $d_1 + d_2 < L$, and $\tilde{F}$ is the electrostatic force expressed as

$$\tilde{F} = \frac{\pi\epsilon_0(V_{dc} + V_{ac}\cos(\tilde{\Omega}\tilde{t}))^2}{\sqrt{(g-\tilde{w})(g-\tilde{w}+2\tilde{R})}(\cosh^{-1}(1+(g-\tilde{w})/\tilde{R}))^2} \tag{2}$$

where ϵ_0 is the dielectric constant of the gap medium. The boundary conditions are:

$$\begin{aligned} &\tilde{w}(0,\tilde{t}) = 0,\ \partial_{\tilde{x}}\tilde{w}(0,\tilde{t}) = 0, \\ &\partial_{\tilde{x},\tilde{x}}\tilde{w}(L,\tilde{t}) = 0,\ \partial_{\tilde{x},\tilde{x},\tilde{x}}\tilde{w}(L,\tilde{t}) = 0 \end{aligned} \tag{3}$$

2.2. Normalization

For convenience, Eq. (1) is normalized. To this end, the following nondimensional variables are introduced:

$$w = \frac{\tilde{w}}{g}, x = \frac{\tilde{x}}{L}, t = \frac{\tilde{t}}{\tau} \tag{4}$$

where τ is a time constant defined by

$$\tau = \sqrt{\frac{\rho A L^4}{EI}}$$

Substitution of Eq. (4) into Eqs. (1) and (3) yields:

$$\begin{aligned} &\partial_{x,x,x,x}w + \partial_{t,t}w + c\partial_t w = \alpha_1 \\ &\partial_x(\partial_x w \partial_x(\partial_x w \partial_{x,x}w)) + \alpha_2\mathcal{H}(x)F \end{aligned} \tag{5}$$

$$\mathcal{H}(x) = H\left(x - \frac{d_1}{L}\right) - H\left(x - 1 + \frac{d_2}{L}\right)$$

$$\begin{aligned} &w(0,t) = 0,\ \partial_x w(0,t) = 0, \\ &\partial_{x,x}w(1,t) = 0,\ \partial_{x,x,x}w(1,t) = 0 \end{aligned} \tag{6}$$

where $d_1 + d_2/L < 1$ and

$$F = \frac{(V_{ac}\cos(\Omega t) + V_{dc})^2}{\sqrt{(1 - w(x,t) + R_2)^2 - R_2^2}\cosh^{-1}\left(\frac{1-w(x,t)}{R_2} + 1\right)^2} \tag{7}$$

Expressions of nondimensional parameters introduced in Eq. (5) are

$$\alpha_1 = \left(\frac{g}{L}\right)^2, \quad \alpha_2 = \frac{\pi\epsilon_0 L^4}{EIg^2}, \quad c = \tilde{c}\frac{L^4}{EI\tau}, \quad \Omega = \frac{\tilde{\Omega}}{\tau}, \quad R_2 = \frac{\tilde{R_2}}{g} \tag{8}$$

2.3. Reduced-order model

In order to eliminate the spatial dependence, the Galerkin decomposition method is applied to Eq. (5) to transform it into multiple degree-of-freedom system. To this end, the beam deflection $w(x,t)$ can be written in this form

$$w(x,t) = \sum_{k=1}^{N_m} a_k(t)\phi_k(x) \tag{9}$$

where N_m is the number of modes retained in the solution, $a_k(t)$ is the kth nondimensional modal coordinate and $\phi_k(x)$ is the kth normalized linear undamped mode shape of a straight beam which is the eigenmode solution of

$$\frac{d^4\phi_k(x)}{dx^4} = \lambda_k^4\phi_k(x) \tag{10}$$

where λ_k is the solution of the transcendental equation

$$1 + \cos(\lambda_k)\cosh(\lambda_k) = 0 \tag{11}$$

To simplify the Galerkin procedure [31], the electrostatic force in Eq. (5) is expanded in a fifth-order Taylor series. The modal projection consists in substituting Eq. (9) into Eq. (5), multiplying the result by $\phi_k(x)$, using Eq. (10) to eliminate $(d^4\phi_k(x))/dx^4$ and integrating the outcome from $x = 0$ to 1. Doing so, Eq. (5) becomes

$$\begin{aligned} &a_i'' + c_i a_i' + \lambda_i^4 a_i + \alpha_1\sum_{j=1}^{N_m}\sum_{k=1}^{N_m}\sum_{l=1}^{N_m}\left(\int_0^1 \phi_i\phi_j\phi_k'\phi_l'\,dx\right)\lambda_j^4 a_j a_k a_l \\ &\quad + \alpha_1\sum_{j=1}^{N_m}\sum_{k=1}^{N_m}\sum_{l=1}^{N_m}\left(\int_0^1 \phi_i\phi_j''\phi_k''\phi_l''\,dx\right)a_j a_k a_l \\ &\quad + 4\alpha_1\sum_{j=1}^{N_m}\sum_{k=1}^{N_m}\sum_{l=1}^{N_m}\left(\int_0^1 \phi_i\phi_j'\phi_k''\phi_l^{(3)}\,dx\right)a_j a_k a_l \\ &\quad = \alpha_2 f(a_i,\phi_i) \quad i \in \{1,\ldots,N_m\} \end{aligned} \tag{12}$$

Eq. (12) can be written in matrix–vector form as

$$\begin{aligned} &M_0 a_i'' + C_0 a_i' + K_0 a_i + \alpha_1[K_T(a) + K_{T1}(a) + K_{T2}(a)]a_i \\ &\quad + \alpha_2[D_0 + D_1(a) + D_2(a)]a_i + \alpha_2[E_1(a) + E_2(a)]T_2(a)a_i = \alpha_2 F1 \end{aligned} \tag{13}$$

where $a(t) = [a_1(t), a_2(t), a_3(t), \ldots, a_{N_m}(t)]^T$. The components of matrices M_0, C_0, K_0, $K_T(a)$, $K_{T1}(a)$, $K_{T2}(a)$, D_0, $D_1(a)$, $D_2(a)$, $E_1(a)$ and $E_2(a)$ are respectively $M_{0ij}, C_{0ij}, K_{0ij}, K_{Tij}, K_{T1ij}, K_{T2ij}, D_{0ij}, D_{1ij}, D_{2ij}$, E_{1ij} and E_{2ij}:

$$\begin{aligned} &M_{0ij} = \delta_{ij} \\ &C_{0ij} = c_i\delta_{ij} \\ &K_{0ij} = \lambda_i^4\delta_{ij} \\ &K_{Tij} = \lambda_i^4\sum_{k=1}^{N_m}\sum_{l=1}^{N_m}\left(\int_0^1 \phi_i\phi_j\phi_k'\phi_l'\,dx \quad a_l a_k\right. \\ &K_{T1ij} = 4\sum_{k=1}^{N_m}\sum_{l=1}^{N_m}\left(\int_0^1 \phi_i\phi_j'\phi_k''\phi_l^{(3)}\,dx \quad a_l a_k\right. \\ &K_{T2ij} = \sum_{k=1}^{N_m}\sum_{l=1}^{N_m}\left(\int_0^1 \phi_i\phi_j''\phi_k''\phi_l''\,dx \quad a_l a_k\right. \\ &D_{0ij} = F_2\left(\int_0^1 \mathcal{H}(x)\phi_i\phi_j\,dx\right. \\ &D_{1ij} = F_3\sum_{k=1}^{N_m}\left(\int_0^1 \mathcal{H}(x)\phi_i\phi_j\phi_k\,dx \quad a_k\right. \\ &D_{2ij} = F_4\sum_{k=1}^{N_m}\sum_{l=1}^{N_m}\left(\int_0^1 \mathcal{H}(x)\phi_i\phi_j\phi_k\phi_l\,dx \quad a_l a_k\right. \\ &E_{1ij} = F_5\sum_{k=1}^{N_m}\left(\int_0^1 \mathcal{H}(x)\phi_i\phi_j\phi_k\,dx \quad a_k\right. \\ &E_{2ij} = F_6\sum_{k=1}^{N_m}\sum_{l=1}^{N_m}\left(\int_0^1 \mathcal{H}(x)\phi_i\phi_j\phi_k\phi_l\,dx \quad a_l a_k\right. \end{aligned} \tag{14}$$

The scalar $T_2(a)$ and the entries of $F1$ are

$$T_2(a) = \sum_{m=1}^{Nm}\sum_{n=1}^{Nm}\left(\int_0^1 \phi_n\phi_m\,dx \quad a_n a_m$$
$$F1_i = F_1\int_0^1 \mathcal{H}(x)\phi_i(x)\,dx \tag{15}$$

where F_1, F_2, F_3, F_4, F_5 and F_6 are the coefficients derived from the Taylor expansion up to the fifth-order and the modal projection of the electrostatic force of Eq. (7).

3. HBM+ANM for periodic solutions

For nonlinear oscillators, it is often required to calculate the periodic solutions of nonlinear differential equations. To this end, the first step consists in transforming the nonlinearities of the original system into quadratic terms. Cochelin and Vergez [47] have proposed this technique in order to apply HBM with many harmonics. It can be a limitation of the method because it is not always easy, for any system, to recast it in polynomial quadratic form. Then, the quadratic recast equations are decomposed into truncated Fourier series by means of the harmonic balance method (HBM). The unknowns, in the final algebraic system, are the Fourier coefficients of the original unknowns. The continuation method (ANM) is applied on the resulting system. Finally, numerical results are derived. We apply this method, described in [47], on our system (5) to obtain the numerical results. Thereafter, a detailed description of the quadratic recast and of the combined technique HBM+ANM is given.

3.1. Quadratic recast

A periodically forced system has this form:

$$\dot{w} = f(t, w, \Omega) \tag{16}$$

where w is a vector of unknowns, f is periodic in t and Ω is a real parameter. To simplify the application of HBM method, the first step is to transform Eq. (16) into a new system where the nonlinearities are at most quadratic polynomials as

$$m(\dot{Z}) = c(t, \Omega) + l(Z) + q(Z, Z) \tag{17}$$

where c is a constant vector with respect to the unknown Z, $l(.)$ is a linear vector with respect to the vector entry and $q(.,.)$ is a quadratic vector linear with respect to both entries.

The following variables are introduced in order to transform Eq. (13) into a quadratic system, as described previously.

$$\begin{aligned}
V &= \dot{a}(sizeN_m)\\
y &= \dot{v}(sizeN_m)\\
K_{tot} &= K_T(a) + K_{T1}(a) + K_{T2}(a)(sizeN_m^2)\\
D_{tot} &= D_1(a) + D_2(a)(sizeN_m^2)\\
E_{tot} &= E_1(a) + E_2(a)(sizeN_m^2)\\
S &= E_{tot}a(sizeN_m)\\
T &= T_2(a)(size1)
\end{aligned} \tag{18}$$

System (13) can be rewritten as

$$\begin{array}{lcl|l|l|l}
\dot{a} &=& 0 & + & v & + & 0\\
\dot{v} &=& 0 & + & y & + & 0\\
0 &=& 0 & + & K_{tot} & + & -K_T(a)-K_{T1}(a)-K_{T2}(a)\\
0 &=& 0 & + & D_{tot}-D_1(a) & + & -D_2(a)\\
0 &=& 0 & + & E_{tot}-E_1(a) & + & -E_2(a)\\
0 &=& 0 & + & S & + & -E_{tot}\,a\\
0 &=& 0 & + & T & + & -T_2(a)\\
0 &=& -\alpha_2 F(1+\cos(\Omega t))^2 & + & M_0\,y + C_0\,v + K_0\,a + D_0\,a & + & \alpha_1 K_{tot}a + D_{tot}a + S\,T
\end{array}$$

$$m(\dot{Z}) = c(t, \Omega) + l(Z) + q(Z, Z) \tag{19}$$

where $Z = (a, v, y, K_{tot}, D_{tot}, E_{tot}, S, T)^T$ is the unknown vector of size $N_{eq} = 4N_m + 3N_m^2 + 1$, c is a constant vector with respect to Z, $l(.)$ and $m(.)$ are linear vectors valued operators with respect to Z, and $q(.,.)$ is a quadratic vector. In our case, $N_{eq} = 8$ corresponding to the number of equations of system (19).

3.2. The harmonic balance method (HBM)

The harmonic balance method is now applied to the system of Eqs. (19). The unknown vector Z is decomposed into Fourier series with H harmonics

$$Z(t) = Z_0 + \sum_{k=1}^{H} Z_{c,k}\cos(k\omega t) + \sum_{k=1}^{H} Z_{s,k}\sin(k\omega t) \tag{20}$$

Then, column vector U, with size $(2H+1)\times Neq$, where Neq is the number of equations in Eq. (19), collects the components of the Fourier series as

$$U = [Z_0^t + Z_{c,1}^t + Z_{s,1}^t + Z_{c,2}^t + \cdots + Z_{c,H}^t + Z_{s,H}^t]^t \tag{21}$$

Substituting Eq. (21) into Eq. (19), collecting the terms of the same harmonic index and neglecting the higher order harmonics, we obtain this set of equations

$$\omega M(U) = C + L(U) + Q(U, U) \tag{22}$$

It contains $(2H+1)\times Neq$ equations for the $(2H+1)\times Neq$ unknowns U. Operators $M(.)$, C, $L(.)$, and $Q(.,.)$ depend only on the operators $m(.)$, c, $l(.)$ and $q(.,.)$ of Eq. (19) and on the number of harmonics H.

3.3. The continuation procedure

From Eq. (22), an algebraic system is obtained

$$R(\mathrm{U}) = 0 \tag{23}$$

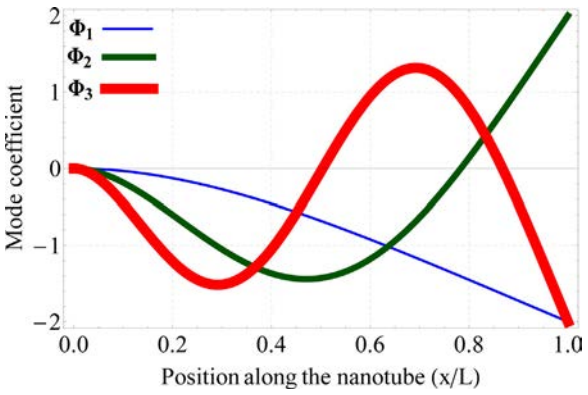

Fig. 2. Shape of the first, second and third bending modes of a carbon nanotube.

where $R \in \mathbb{R}^{N+1}$ and $\mathrm{U} = \left[U^t, \Omega, \omega\right] \in \mathbb{R}^{N+1}$. The Asymptotic numerical method (ANM), which is based on the quadratic recasting, is applied to Eq. (22) to obtain

$$R(\mathrm{U}) = L0 + L(\mathrm{U}) + Q(\mathrm{U}, \mathrm{U}) \tag{24}$$

where $L0$, $L(.)$ and $Q(.,.)$ are respectively constant, linear and bilinear vectors. Then, the solutions are obtained by considering the branches of solution as power series. Indeed, if U_0 is a point solution, the branch passing by U_0 is a power series expansion of the path parameter $a = (\mathrm{U} - \mathrm{U}_0)^t \mathrm{U}_1$, where U_1 is the tangent vector at U_0 and $\mathrm{U}(a) = \mathrm{U}_0 + a\mathrm{U}_1 + a^2\mathrm{U}_2 + a^3\mathrm{U}_3 + \cdots + a^n\mathrm{U}_n$. This series is replaced in Eq. (23) where the powers of a are equated to zero providing a set of linear systems.

4. Results and discussions

Using the HBM+ANM procedure, we plot the frequency-amplitude diagrams of the carbon nanotube for several parameter designs. Fig. 2, representing the first three bending modes with respect to the dimensionless position x/L, shows that the problem is not symmetric, where Φ_i, $i \in \{1, 2, 3\}$, is the ith linear undamped bending mode shape of the carbon nanotube. Hence, both odd and even modes are considered.

Due to the kind of the dominant nonlinearities, the even harmonics have no influence. In addition and after verifications, the first harmonic gives the most important informations. So, in our case, we have plotted the amplitudes W_{max-i}, $i \in \{1, 2, 3\}$, of the first three modes normalized by the gap g at $x = L$ and corresponding to the first harmonic. Two oscillator designs, listed in Table 1, having the same quality factor $Q = 5000$ and representing different behaviors, are considered in order to show the impact of each mode on the frequency responses and to retain the most appropriate number of used modes.

The HBM+ANM technique is used to extract the dynamic responses of the first three modes when using one, two or three modes in the reduced-order model. The solution is computed with $H = 5$ harmonics for the HBM and $N_m = 3$ modes for the Galerkin procedure. For the following investigations, the electrode is placed at $d_1/L = d_2/L = 0.3$. Consequently, the maximum amplitude $W_{max} = W_{max-1} + W_{max-2} + W_{max-3} \approx W_{max-1}$ is equal to $|\Phi_{1(1)}/2\Phi_{1(0.7)}| \approx 84.62\,\%$ of the gap g.

Table 1
Design parameters of investigated resonators.

Resonator	$L(\mu m)$	$R_1(nm)$	$R_2(nm)$	$g(nm)$
1	1	10	20	100
2	20	180	300	100

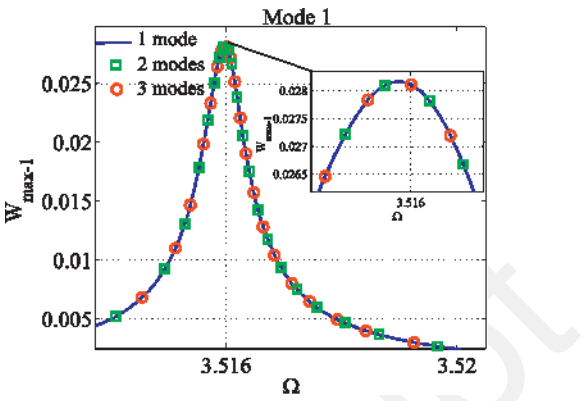

Fig. 3. Confrontation of the frequency responses of the first mode obtained for one, two and three modes of a linear configuration.

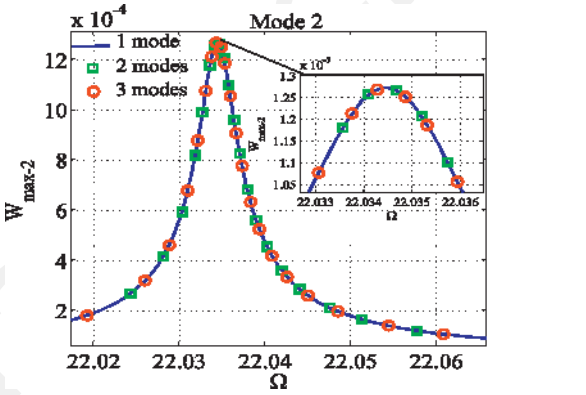

Fig. 4. Confrontation of the frequency responses of the second mode obtained for one, two and three modes of a linear configuration.

Initially, numerical simulations have been performed to track the frequency responses of the first nanotube in Table 1 under a moderate electrostatic force ($V_{ac} = 0.4V$, $V_{dc} = 5V$) in order to conserve a linear dynamics. The confrontation is shown in Fig. 3 for this configuration when using one or several modes. The frequency responses of the two first modes are depicted in Figs. 3 and 4 with one, two and three modes. Fig. 5 represents the frequency response of the third mode with one and three modes. Particularly, at this linear level, the results are identical independently of the number of retained modes. Indeed, for a linear configuration, the nonlinear terms of Eq. (5) are negligible which implies that the finite degree of freedom system (12), obtained by Galerkin discretization, is uncoupled. Consequently, for this particular case, one mode is

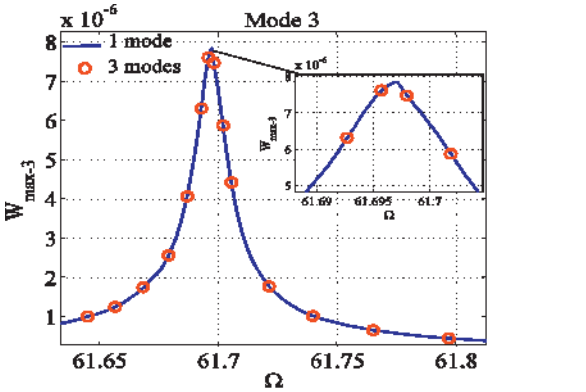

Fig. 5. Confrontation of the frequency responses of the third mode obtained for one and three modes of a linear configuration.

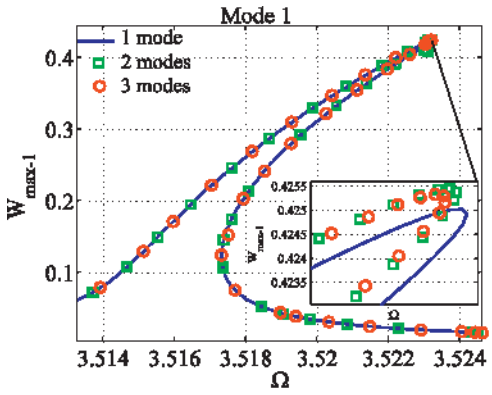

Fig. 6. Confrontation of the frequency responses of the first mode obtained for one, two and three modes of a hardening behavior. The response corresponding to the use of one mode is slightly different.

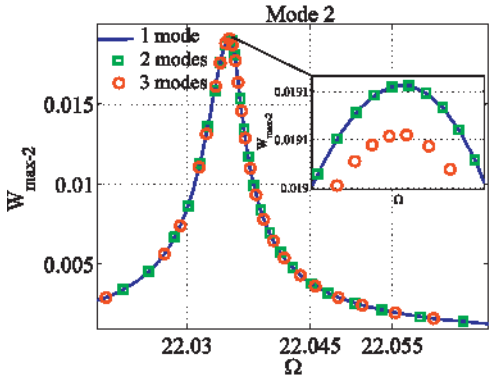

Fig. 7. Confrontation of the frequency responses of the second mode obtained for one and two modes of a hardening configuration. The response corresponding to the use of three modes is slightly different.

sufficient to describe the dynamical behavior of the considered nanotube.

Then, investigations are conducted on the same nanotube design driven at large displacements. To do so, the electrostatic force amplitude is increased significantly ($V_{ac} = 2$ V, $V_{dc} = 15$ V). At this actuation level, the resonator exhibits hardening frequency responses, since the external radius R_2 of the nanotube is much lower than the gap g ($R_2/g = 0.2 < 1$). In this case, as shown in Fig. 6 the responses of the first mode, when using one, two or three modes, are noticeably different and this is due to the amplification of the coupling nonlinear terms. Nevertheless, the variations between the different curves are very slight. They are below 0.05%

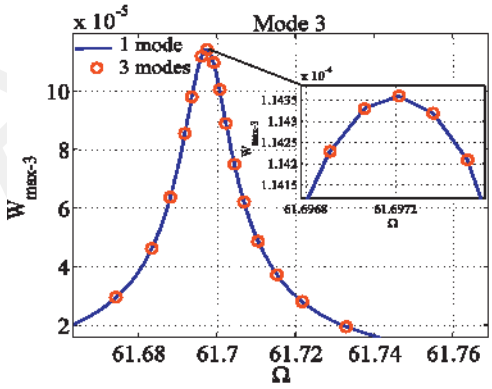

Fig. 8. Confrontation of the frequency responses of the third mode obtained for one and three modes of a hardening configuration.

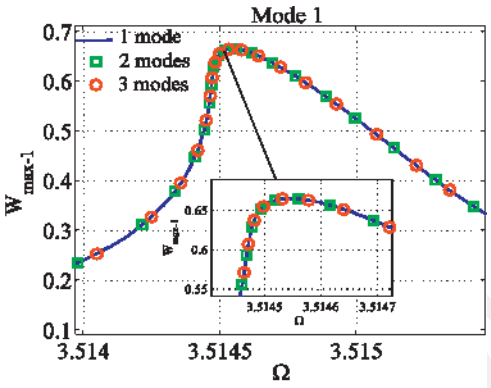

Fig. 9. Confrontation of the frequency responses of the first mode obtained for one, two and three modes of a softening configuration.

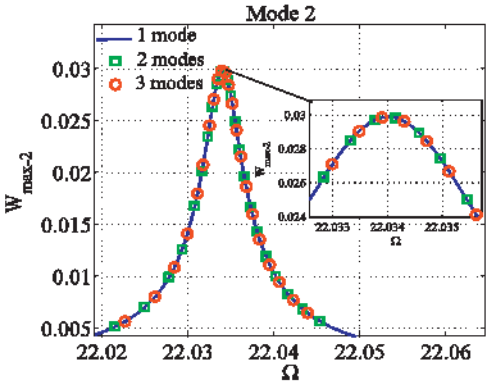

Fig. 10. Confrontation of the frequency responses of the second mode obtained for one, two and three modes of a softening configuration.

in peak amplitude and a negligible shift frequency, which are lower than 5% in peak amplitude [48] and less than 0.5% in frequency due to imperfections in micromachining or to residual stress [49].

Finally, in order to confirm the previous deductions, the same investigations are made on a different oscillator presented by design 2 in Table 1 where $V_{ac} = 1V$ and $V_{dc} = 10V$. This device has a narrow gap with respect to the nanotube radius ($R_2/g = 3 > 1$) which gives rise to the softening behavior. Figs. 9–11, display the confrontation of the frequency responses with one or several modes. The same conclusions as before can be reported concerning the accuracy.

For each design parameters, the number of equations required for the HBM+ANM procedure, for each mode, is $(2 * H + 1) * N_{eq} =$

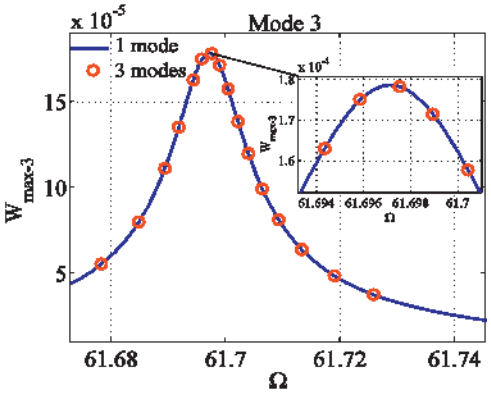

Fig. 11. Confrontation of the frequency responses of the third mode obtained for one and three modes of a softening configuration.

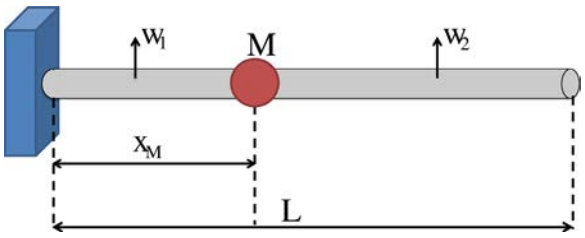

Fig. 12. Schematic of an electrostatically actuated carbon nanotube with an added mass.

88 where $H = 5$ and $N_{eq} = 8$. The HBM+ANM provides relatively fast and precise results. We have shown the impact of the number of the used modes on several configurations. As a conclusion, we can consider a single mode in our investigations, since it gives accurate results concerning the dynamics of the nanotube at large displacements.

5. Resonant mass sensing

The principle of the mass sensing, based on the frequency shift technique, consists on the measurement of the shift of the frequency resulted by an accreted mass at a cantilever. Naik et al. [14], Lavrik and Datskos [3], Yang et al. [5] and Verd et al. [4] have detected the mass of several particles by using this technique. Their investigations were done with resonators having linear behavior. To our knowledge, it is the first time that a carbon nanotube actuated electrostatically, having a nonlinear behavior and with a specific position of the electrode is investigated for mass sensing applications. The resonant sensing technique is used in order to derive the frequency shifts of the maximum amplitudes (Fig. 13) for several added particles.

5.1. Bending modes

In the left and right regions of the attached mass (Fig. 12,), the bending mode is decomposed into $w_{1,n}(x, t)$ and $w_{2,n}(x, t)$, where n is the considered mode, subject to the differential equation (5).

At the mass location $\delta_M = x_M/L$, the corresponding matching conditions are:

$$w_{1,n}(\delta_M, t) = w_{2,n}(\delta_M, t), \quad w_{1,n}{}'(\delta_M, t) = w_{2,n}{}'(\delta_M, t), \quad w_{1,n}{}''(\delta_M, t) = w_{2,n}{}''(\delta_M, t)$$
$$EI(w_{1,n}{}'''(\delta_M, t) - w_{2,n}{}'''(\delta_M, t)) = M\ddot{w}_{2,n}(\delta_M, t) \tag{25}$$

and the boundary conditions at the clamped and the free extremities are:

$$w_{1,n}(0, t) = 0, w_{1,n}{}'(0, t) = 0,$$
$$w_{2,n}{}''(1, t) = 0, w_{2,n}{}'''(1, t) = 0 \tag{26}$$

The transversal displacements on the two parts of the nanotube are $w_{i,n}(x, t) = \Phi_{i,n}(x)\cos(\omega_n t - \phi)$, $i \in \{1, 2\}$, where ω_n is the natural frequency of the nth mode, yielding to the following linear undamped bending modes

$$\Phi_{1,n}(\delta_x) = A_1\cos(\lambda_n\delta_x) + A_2\sin(\lambda_n\delta_x) + A_3\cosh(\lambda_n\delta_x) + A_4\sinh(\lambda_n\delta_x), \delta_x \in \left[0, \frac{x_M}{L}\right]$$
$$\Phi_{2,n}(\delta_x) = A_5\cos(\lambda_n\delta_x) + A_6\sin(\lambda_n\delta_x) + A_7\cosh(\lambda_n\delta_x) + A_8\sinh(\lambda_n\delta_x), \delta_x \in \left[\frac{x_M}{L}, 1\right] \tag{27}$$

where λ_n is the nth natural frequency of the mechanical structure, $A_i, i \in \{1, \ldots, 8\}$ are integration constants determined from the matching and boundary conditions for $w_{1,n}$ and $w_{2,n}$, respectively Eqs. (25) and (26). These constants are obtained by equating the corresponding determinant of coefficients to zero. The determinant equation includes the following nondimensional parameters

$$\delta_x = \frac{x}{L}, \quad \delta_M = \frac{M}{\rho AL}, \quad \lambda_n = \frac{\omega_n^4\rho AL^4}{EI} \tag{28}$$

where ω_n is the natural frequency corresponding to the nth mode, x is the coordinate along the beam and $\delta_M = M/M_{CNT}$ is the mass ratio between the weights of a particle and of the CNT, respectively M and M_{CNT}.

5.2. Determination of the mass and the position of an added particle

Despite the fact that a single mode provides very precise frequency responses, as demonstrated previously, it is not sufficient for mass sensing applications. Indeed, one mode defines only one equation, while an added particle is identified by two unknowns: the mass and the position. Thus, at least two modes must be used to derive two equations which can be effectively solved. Nevertheless, Fig. 2 shows that the second mode has a node approximately at $x/L = 0.8$ for which the resonator has no response. Thus, it is impossible to obtain the mass of a particle placed at this specific position by using only two modes. Consequently, three modes, at least, are necessary for an efficient mass detection. That is why, hereafter, the numerical simulations are performed on a three degree of freedom reduced-order model considering only the three first bending modes.

The frequency responses of the CNT are investigated for the first design parameters of Table 1 ($L = 1\ \mu$m, g = 100 nm, $V_{dc} = 15$ V, $V_{ac} = 2$ V, $Q = 5000$, $R_1 = 10$ nm, $R_2 = 20$ nm and $d_1 = d_2 = 0.3$), producing a hardening behavior ($R_2/g = 0.2 < 1$). For ten values of $\delta_x \in [0.1, 1]$ and ten values of $\delta_M \in [0.01, 2](\%)$, 300 frequency responses of the first three modes are plotted using the HBM+ANM procedure. Fig. 13 shows the frequency responses of the first mode of the nanotube for the particular case of an added particle at the position $\delta x = 0.9$ and for ten values of δM. The ultimate goal is to derive the frequency shifts δf_{i-NL}, represented by Eq. (29), between the $f_{i,M}$ (peak frequency with added mass) and the resonance frequency of the CNT without added mass f_i for each mode ($i \in \{1, 2, 3\}$). A shift is illustrated in Fig. 13, δf_{2-NL}, corresponding to a mass ratio $\delta M = 1\%$ placed at $\delta x = 0.9$.

$$\delta f_{i-NL} = \frac{f_i - f_{i,M}}{f_i}, i \in \{1, 2, 3\} \tag{29}$$

Firstly, for each mode and for the different values of δ_x and δ_M, we compute analytically the bending modes $\Phi_{1,i}(x)$ and $\Phi_{2,i}(x)$ and the natural frequencies λ_i and $\lambda_{i,\delta x,\delta M}$, for the ith mode of the CNT respectively without and with added particle at δx and having a mass ratio δM. The frequency shifts of linear and nonlinear

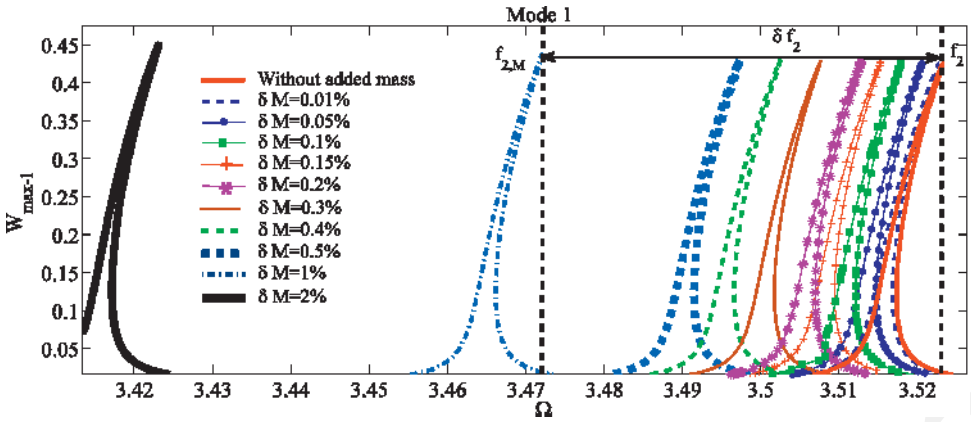

Fig. 13. Frequency responses of the carbon nanotube of the first mode for $\delta x = 0.9$ and for ten different values of δM ($\delta_M \in [0.01, 2](\%)$). δf_{2-NL} is the frequency shift between the two resonance peaks of the nanotube, respectively, without and with added mass $\delta M = 1\%$ at the position $\delta x = 0.9$.

configurations are derived separately. For the linear case, the shifts are obtained directly by using the following formula

$$\delta f_{i-L} = \frac{\lambda_i^2 - \lambda_{i,\delta x,\delta M}^2}{\lambda_i^2}, i \in \{1, 2, 3\} \tag{30}$$

However, for the nonlinear case, a numerical method should be used in order to detect the peak amplitudes of the nonlinear curves. Practically, the modal projection is applied on Eq. (5) using the first three modes defined as piecewise functions in Eq. (27). Then, the steady state periodic solutions of the three-degree-of-freedom system are determined numerically using the harmonic balance method (HBM) transforming the coupled differential equations into a system of coupled nonlinear algebraic equations. The resulting system is solved using the asymptotic numerical method (ANM). Doing so, the branches of the nonlinear frequency responses can be extracted and the peak amplitudes can be automatically tracked. The shifts δf_{i-NL} are evaluated for each peak amplitude. Finally, the maps representing the frequency shifts, computed for linear and nonlinear configurations, are plotted as a function of δx and δM for the three first modes.

The maps of the frequency shifts of the first mode are depicted in Fig. 14(a) and (b) respectively for the linear and the nonlinear configurations. For the linear case, the maximum shift is obtained for a particle placed at the extremity of the nanotube ($\delta x = 1$) and for the highest mass ratio ($\delta M = 2\%$). In fact, as shown in Fig. 2, the largest value of the mode is obtained at the free end of the resonator (for $x/L = 1$, $|\Phi_1(1)| = 2$) and the beam deflection $w(x, t)$ is written as a function of the mode (Eq. (9)). So, for higher values of δx, the frequency responses are largely shifted with respect to the resonance frequency of the CNT without added mass. Analogically, the same remarks can be reported for the lowest shift corresponding to the couple ($\delta x = 0.1, \delta M = 0.01\%$).

The nonlinear configuration is illustrated by Fig. 14(b). Identical frequency shifts are identified between the linear and the nonlinear cases for $\delta x \in [0.7, 1]$ or $\delta M \in [0.01\,\%, 0.4\,\%]$. The rest of the maps are remarkably different. The pronounced spring hardening effect in the frequency responses of the first mode are at the origin of these differences, as depicted in Fig. 14.

Similarly to the first mode, the second mode has the highest and the lowest shifts for the same values of δx and δM (Fig. 15(a) and (b)). Notably, the maps of the linear and the nonlinear configurations are perfectly similar for the second and third modes (Figs. 15 and 16) which is due to the fact that the frequency responses are linear as shown in Figs. 7 and 8. Hence, the analytical expression of the shift (Eq. (30)) can be used as in the linear case for the second and third modes in order to reduce considerably the computational time. Moreover, Fig. 16(a) and (b) depict dark columns for δx equal to 0.5 and to 0.9. Indeed, Fig. 2 shows that the shape of the third mode intersects the x-axis in two points near the positions 0.5 and 0.9, for which, the peak amplitude of the NEMS frequency response around the considered bending mode is null.

From the frequency shift maps of the first mode, we can determine the mass and the position of a particle based on the frequency shifts. But, this method is no longer valid if different particles admit the same value of the shift. For instance, using Fig. 14 (a), the two cases $c_1 = (\delta x = 0.6, \delta M = 0.05\,\%)$ and $c_2 = (\delta x = 0.4, \delta M = 0.2\,\%)$ have the same frequency shift ($\delta f = 0.0021$). Thus, the effective added mass cannot be identified by simply using only the first mode. The alternative is to use the shifts for the linear configuration of the second mode depicted in Fig. 15 (a). The two couples c_1 and c_2 have respectively $s_1 = 0.0181$ and $s_2 = 0.0104$ which are different. Therefore, the exact added mass is determined using the frequency shift maps of the second mode.

Unlike Fig. 14 of the first mode, the maps of Fig. 15 show a dark column for $\delta x = 0.8$ representing very low frequency shifts. This describes that the CNT has small deflection in this position. Effectively, in Fig. 2, the shape of the second mode intersects the mode coefficient axis in a position near $x/L = 0.8$. It corresponds to a null coefficient of the mode for which the resonator is insensitive to any added mass. Consequently, the mass and position of an added particle at $\delta x \approx 0.8$ cannot be determined using only two modes. This issue can be illustrated by the cases $c_3 = (\delta x = 0.8, \delta M = 0.0001)$ and $c_4 = (\delta x = 0.4, \delta M = 0.001)$ in Fig. 14(a) for which we have the same frequency shift equal to 0.000105. The data displayed in Fig. 15(a) is therefore used in order to find the correct position and mass of the added particle. We observe that for c_3, the value of the frequency shift is almost null (9.8×10^{-7}) while it is equal to 0.00093 for c_4. These data do not provide reliable results, because, the frequency shift of c_3 corresponding to the second mode is very small. Therefore, one cannot conclude whether c_3 or c_4 is the correct solution. In order to avoid this issue, the frequency shift map of the third mode is used (Fig. 16(a)). It gives two different results, $s_3 = 0.000031$ and $s_4 = 0.000055$ respectively for c_3 and c_4. Based on s_3 and s_4, the correct solution can be identified.

As synthesis, there are strong similarities between the linear and the nonlinear maps corresponding to the second and the third modes (Figs. 15 and 16). This can be explained by the simple fact that the frequency responses of both second and third modes are linear. Consequently, the frequency shifts can be computed directly by using their analytical formulas. Inversely, the linear and nonlinear configurations of the first mode (Fig. 14(a) and (b)) have several differences, and then for this particular case, the use of the HBM+ANM procedure is essential. Concretely, a hybrid

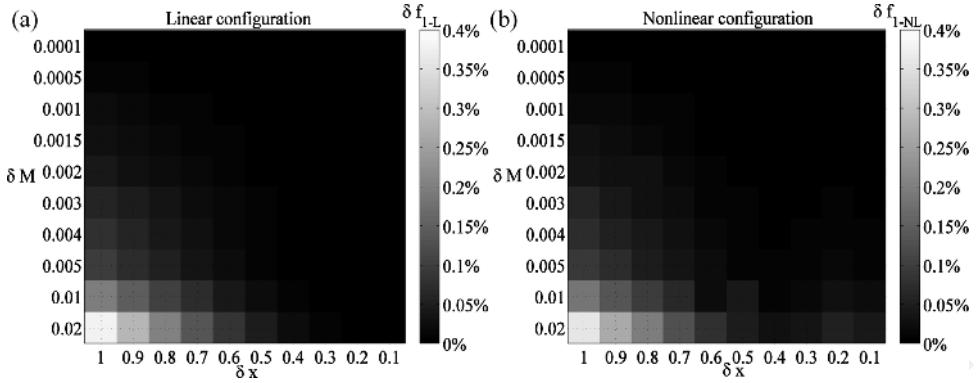

Fig. 14. Frequency shifts of the first mode for the design parameters $L = 1\,\mu m$, $g = 100$ nm, $Q = 5000$, $R_1 = 10$ nm, $R_2 = 20$ nm and $d_1/L = d_2/L = 0.3$ for (a) a linear configuration subject to a moderate electrostatic force ($V_{dc} = 5$ V, $V_{ac} = 0.4$ V) and (b) a nonlinear hardening behavior under a high electrostatic actuation ($V_{dc} = 15$ V, $V_{ac} = 2$ V). In each case, these frequency shifts are derived for ten values of the position ratio $\delta_x = x_M/L \in [0.1, 1]$ and ten values of the mass ratio $\delta_M = M/M_{CNT} \in [0.01, 2](\%)$. The minimum frequency shift is obtained for a particle placed close to the clamped end of the nanotube ($\delta x = 0.1$) and for the lowest mass ratio ($\delta M = 0.01\%$) while the maximum one is obtained for $\delta x = 1$ and $\delta M = 2\%$. The maps for the linear and the nonlinear cases, respectively (a) and (b), have several differences, except in the intervals $\delta x \in [0.7, 1]$ or $\delta M \in [0.01\%, 0.4\%]$ wherein they are perfectly identical.

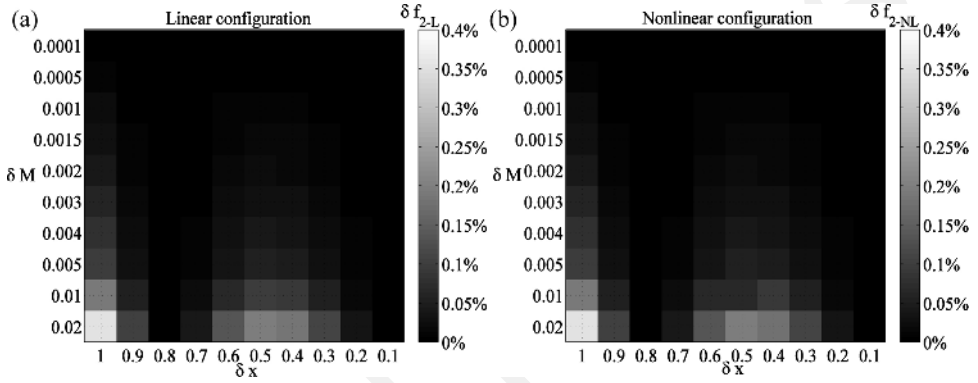

Fig. 15. Frequency shifts of the second mode for the design parameters $L = 1\,\mu m$, $g = 100$ nm, $Q = 5000$, $R_1 = 10$ nm, $R_2 = 20$ nm and $d_1/L = d_2/L = 0.3$ for (a) a linear configuration subject to a moderate electrostatic force ($V_{dc} = 5V$, $V_{ac} = 0.4$ V) and (b) a nonlinear hardening behavior under a high electrostatic actuation ($V_{dc} = 15$ V, $V_{ac} = 2$ V). In each case, these frequency shifts are derived for ten values of the position ratio $\delta_x = x_M/L \in [0.1, 1]$ and ten values of the mass ratio $\delta_M = M/M_{CNT} \in [0.01, 2](\%)$, where M_{CNT} is the mass of the carbon nanotube. The maps for the linear and the nonlinear cases, respectively (a) and (b), are perfectly identical for all values of δM and δx. Consequently, the frequency shifts of the second mode corresponding to the nonlinear configuration can be derived by directly using the analytical expression of Eq. (30).

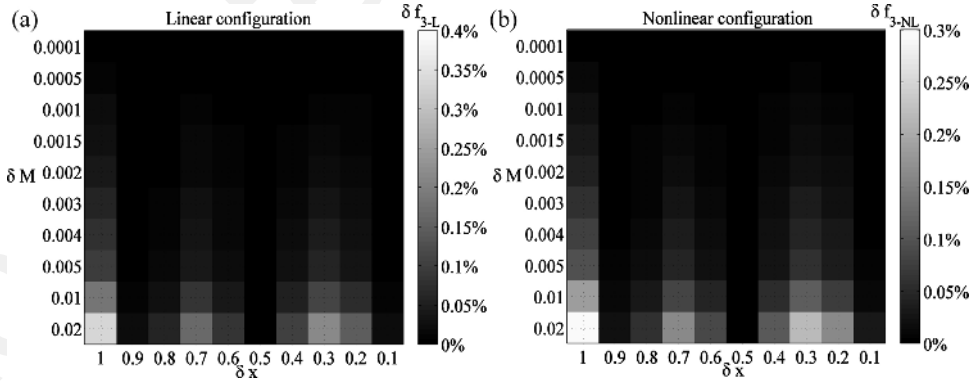

Fig. 16. Frequency shifts of the third mode for the design parameters $L = 1\,\mu m$, $g = 100$ nm, $Q = 5000$, $R_1 = 10$ nm, $R_2 = 20$ nm and $d_1/L = d_2/L = 0.3$ for (a) a linear configuration subject to a moderate electrostatic force ($V_{dc} = 5$ V, $V_{ac} = 0.4$ V) and (b) a nonlinear hardening behavior under a high electrostatic actuation ($V_{dc} = 15$ V, $V_{ac} = 2$ V). In each case, these frequency shifts are derived for ten values of the position ratio $\delta_x = x_M/L \in [0.1, 1]$ and ten values of the mass ratio $\delta_M = M/M_{CNT} \in [0.01, 2](\%)$, where M_{CNT} is the mass of the carbon nanotube. The maps for the linear and the nonlinear cases, respectively (a) and (b), are perfectly identical for all values of δM and δx. Consequently, the frequency shifts of the third mode corresponding to the nonlinear configuration can be derived by directly using the analytical expression of Eq. (30).

analytical–numerical approach can be used in order to reduce the computational time. In practice, we can obtain larger maps for the three modes giving a wide range of configurations of added particles. It is also possible to investigate analytically the frequency shifts of higher modes in order to provide more precise results.

6. Conclusion

In this paper, the nonlinear dynamics of a cantilevered carbon nanotube actuated under primary resonance and including geometric and electrostatic nonlinearities was modeled. The

Euler–Bernoulli partial differential equation describing the nonlinear motion of the resonator is transformed into a system of coupled nonlinear ordinary differential equations using the Galerkin decomposition method.

Firstly, we developed a numerical multimodal approach based on the harmonic balance method (HBM) and the asymptotic numerical method (ANM). It was demonstrated, for several design parameters, that the use of a single mode is sufficient to capture the main nonlinear phenomena of the considered device. Nevertheless, for mass detection, it is required to work at least with three modes. Indeed, it was shown by means of the mode shapes that, for particular positions along the nanotube length, certain mode coefficients are null. Thus, the device has no response and it is insensitive to any added particle. Therefore, a reduced-order model considering three modes was developed.

Then, because the detection of the position and the mass of a particle demands very sophisticated mathematical tools, we have treated this problem in an inverse way. Indeed, for a particular nonlinear design, we derived the frequency shifts corresponding to several positions and with different masses. A specific Galerkin procedure based on piecewise functions is used, combined with the HBM+ANM for the numerical computation of the frequency responses. In these investigations, we have demonstrated that the use of at least three modes is essential to determine effectively the mass and position of the added particle. In fact, two different particles can give the same frequency shift for the first mode. So, the second mode is used to avoid this problem. However, the position of the particle on the nanotube can potentially coincide with the node of the second mode for which the resonator has no response. Consequently, the use of the third mode is essential in order to detect effectively the mass and the position of the added mass. The maps of the frequency shifts for the two cases of linear and nonlinear devices and for the second and third modes are particularly identical. This is explained by the fact that the responses of these two modes are linear. For these cases, an analytical approach can be used to determine the frequency shifts. Unlike the second and the third mode, the response of the first mode exhibits a nonlinear behavior. Thus, the maps of the frequency shifts corresponding to linear and nonlinear oscillators are different. For this case, the HBM+ANM procedure is applied. In practice, the use of a hybrid analytical–numerical approach provides larger frequency shift maps to deal efficiently with the resonant mass sensing technique while keeping an acceptable accuracy with respect to the device resolution.

Acknowledgment

This project has been performed in cooperation with the Labex ACTION program (contract ANR-11-LABX-01-01).

References

[1] M.L. Roukes, Nanoelectromechanical systems face the future, Physics World 14 (2001) 25.
[2] K.L. Ekinci, X.M.H. Huang, M.L. Roukes, Ultrasensitive nanoelectromechanical mass detection, Applied Physics Letters 84 (2004) 4469–4471.
[3] N.V. Lavrik, P.G. Datskos, Femtogram mass detection using photothermally actuated nanomechanical resonators, Applied Physics Letters 82 (2003) 2697–2699.
[4] J. Verd, A. Uranga, G. Abadal, J. Teva, F. Torres, F. Perez-Murano, J. Fraxedas, J. Esteve, N. Barniol, Monolithic mass sensor fabricated using a conventional technology with attogram resolution in air conditions, Applied Physics Letters 91 (2007) 013501.
[5] Y.T. Yang, C. Callegari, X.L. Feng, K.L. Ekinci, M.L. Roukes, Zeptogram-scale nanomechanical mass sensing, Nano Letters 6 (2006) 583–586.
[6] I. Stachiv, A.I. Fedorchenko, Y.L. Chen, Mass detection by means of the vibrating nanomechanical resonators, Applied Physics Letters 100 (2012) 093110.
[7] M.S. Hanay, S. Kelber, A.K. Naik, D. Chi, S. Hentz, E.C. Bullard, E. Colinet, L. Duraffourg, M.L. Roukes, Single-protein nanomechanical mass spectrometry in real time, Nature Nanotechnology 7 (2012) 602–608.
[8] M. Thompson, D.C. Stone, in: J.D.W. Inefordner (Ed.), Surface-Launched Acoustic Wave Sensors: Chemical Sensing and Thin-Film Characterization, Wiley, New York, 1997.
[9] T. Thundat, S.L. Sharp, W.G. Fisher, R.J. Warmack, E.A. Wachter, Micromechanical radiation dosimeter, Applied Physics Letters 66 (1995) 1563–1565.
[10] C. Lu, A.W. Czanderna, Applications of Piezoelectric Quartz Crystal Microbalances, Elsevier, New York, 1984.
[11] B. Ilic, H.G. Craighead, S. Krylov, W. Senaratne, C. Ober, P. Neuzil, Attogram detection using nanoelectromechanical oscillators, Journal of Applied Physics 95 (2004) 3694–3703.
[12] E.H. Feng, R.E. Jones, Carbon nanotube cantilevers for next-generation sensors, Physical Review B 83 (2011) 195412.
[13] H.M. Ouakad, M.I. Younis, Nonlinear dynamics of electrically actuated carbon nanotube resonators, ASME Journal of Computational and Nonlinear Dynamics 5 (2010) 1–13.
[14] A.K. Naik, M.S. Hanay, W.K. Hiebert, X.L. Feng, M.L. Roukes, Towards single-molecule nanomechanical mass spectrometry, Nature Nanotechnology 4 (2009) 445–450.
[15] B. Domon, R. Aebersold, Mass spectrometry and protein analysis, Science 312 (2006) 212–217.
[16] R. Aebersold, M. Mann, Mass spectrometry based proteomics, Nature 422 (2003) 198–207.
[17] M. Kohler, W. Fritzsche, Nanotechnology: An Introduction to Nanostructuring Techniques, Wiley-VCH, Germany, 2004.
[18] H.S. Wasisto, S. Merzsch, A. Stranz, A. Waag, E. Uhde, T. Salthammer, E. Peiner, Femtogram aerosol nanoparticle mass sensing utilising vertical silicon nanowire resonators, Micro and Nano Letters, IET 8 (2013) 554–558.
[19] K.L. Ekinci, Y.T. Yang, M.L. Roukes, Ultimate limits to inertial mass sensing based upon nanoelectromechanical systems, Journal of Applied Physics 95 (2004) 2682–2689.
[20] K. Jensen, K. Kim, A. Zettl, An atomic-resolution nanomechanical mass sensor, Nature Nanotechnology 3 (2008) 533–537.
[21] H.Y. Chiu, P. Hung, H.W.C. Postma, M. Bockrath, Atomic-scale mass sensing using carbon nanotube resonators, Nano Letters 8 (2008) 4342–4346.
[22] B. Lassagne, D. Garcia-Sanchez, A. Aguasca, A. Bachtold, Ultrasensitive mass sensing with a nanotube electromechanical resonator, Nano Letters 8 (2008) 3735–3738.
[23] R. Lifshitz, M.C. Cross, in: H.G. Schuster (Ed.), Review of Nonlinear Dynamics and Complexity, Wiley-VCH, Weinheim, 2008.
[24] A.N. Cleland, M.L. Roukes, External control of dissipation in a nanometer-scale radiofrequency mechanical resonator, Sensors and Actuators A: Physical 72 (1999) 256–261.
[25] L.G. Villanueva, E. Kenig, R.B. Karabalin, M.H. Matheny, R. Lifshitz, M.C. Cross, M.L. Roukes, Surpassing fundamental limits of oscillators using nonlinear resonators, Physical Review Letters 110 (2013) 177208.
[26] N. Kacem, S. Hentz, Bifurcation topology tuning of a mixed behavior in nonlinear micromechanical resonators, Applied Physics Letters 95 (2009) 3.
[27] N. Kacem, S. Hentz, D. Pinto, B. Reig, V. Nguyen, Nonlinear dynamics of micro/nanomechanical beam resonators: improving the performance of NEMS-based sensors, Nanotechnology 20 (2009) 11.
[28] A.H. Nayfeh, M.I. Younis, E.M. Abdel-Rahman, Dynamic pull-in phenomenon in MEMS resonators, Nonlinear Dynamics 48 (2007) 153–163.
[29] M.I. Younis, E.M. Abdel-Rahman, A.H. Nayfeh, A reduced-order model for electrically actuated microbeam-based MEMS, Journal of Microelectromechanical Systems 12 (2003) 672–680.
[30] M.I. Younis, A.H. Nayfeh, A study of the nonlinear response of a resonant microbeam to an electric actuation, Nonlinear Dynamics 31 (2003) 91–117.
[31] W.C. Xie, H.P. Lee, S.P. Lim, Nonlinear dynamic analysis of MEMS switches by nonlinear modal analysis, Nonlinear Dynamics 31 (2003) 243–256.
[32] V. Rochus, D.J. Rixen, J.-C. Golinval, Electrostatic coupling of MEMs structures: transient simulations and dynamic pull-in, Nonlinear Analysis 63 (2005) 1619–1633.
[33] J. Fritz, M.K. Baller, H.P. Lang, H. Rothuizen, P. Vettiger, E. Meyer, H.-J. Guntherodt, C. Gerber, J.K. Gimzewski, Translating biomolecular recognition into nanomechanics, Applied Physics Letters 288 (2000) 316–318.
[34] E. Forsen, G. Abadal, S. Ghatnekar-Nilsson, J. Teva, J. Verd, R. Sandberg, W. Svendsen, F. Perez-Murano, J. Esteve, E. Figueras, F. Campabadal, L. Montelius, N. Barniol, A. Boisen, Ultrasensitive mass sensor fully integrated with complementary metal oxide semiconductor circuitry, Applied Physics Letters 87 (2005) 043507.
[35] N. Kacem, J. Arcamone, F. Perez-Murano, S. Hentz, Dynamic range enhancement of nonlinear nanomechanical resonant cantilevers for highly sensitive NEMS gas/mass sensor applications, Journal of Micromechanics and Microengineering 20 (2010) 045023.
[36] H.B. Peng, C.W. Chang, S. Aloni, T.D. Yuzvinsky, A. Zettl, Ultrahigh frequency nanotube resonators, Physical Review Letters 97 (2006) 087203.
[37] S. Dohn, O. Hansen, A. Boisen, Cantilever based mass sensor with hard contact readout, Applied Physics Letters 88 (2006) 264104.
[38] T.P. Burg, S.R. Manalis, Suspended microchannel resonators for biomolecular detection, Applied Physics Letters 83 (2003) 2698–2700.
[39] B. Reulet, A.Y. Kasumov, M. Kociak, R. Deblock, I.I. Khodos, Y.B. Gorbatov, V.T. Volkov, C. Journet, H. Bouchiat, Acoustoelectric effects in carbon nanotubes, Physical Review Letters 85 (2000) 2829–2832.
[40] S.T. Purcell, P. Vincent, C. Journet, V.T. Binh, Tuning of nanotube mechanical resonances by electric field pulling, Physical Review Letters 89 (2002) 276103.

[41] V. Sazonova, Y. Yaish, H. Ustunel, D. Roundy, T.A. Arias, P.L. Mceuen, A tunable carbon nanotube electromechanical oscillator, Nature 431 (2004) 284–287.
[42] J. Teva, G. Abadal, F. Torres, J. Verd, F. Perez-Murano, N. Barniol, A femtogram resolution mass sensor platform based on SOI electrostatically driven resonant cantilever. Part II: sensor calibration and glycerine evaporation rate measurement, Ultramicroscopy 106 (2006) 808–814.
[43] S. Dohn, R. Sandberg, W. Svendsen, A. Boisen, Enhanced functionality of cantilever based mass sensors using higher modes, Applied Physics Letters 86 (2005) 233501.
[44] S. Dohn, W. Svendsen, A. Boisen, O. Hansen, Mass and position determination of attached particles on cantilever based mass sensors, Review of Scientific Instruments 78 (2007) 103303.
[45] P.R. Sethna, Vibrations of dynamical systems with quadratic nonlinearities, Journal of Applied Mechanics 32 (1965) 576–582.
[46] E. Mile, G. Jourdan, I. Bargatin, S. Labarthe, C. Marcoux, P. Andreucci, S. Hentz, C. Kharrat, E. Colinet, L. Duraffourg, In-plane nanoelectromechanical resonators based on silicon nanowire piezoresistive detection, Nanotechnology 21 (2010) 165504.
[47] B. Cochelin, C. Vergez, A high order purely frequency-based harmonic balance formulation for continuation of periodic solutions, Journal of Sound and Vibration 324 (2009) 243–262.
[48] V. Sazonova, A tunable carbon nanotube resonator, Cornell University, Ithaca, NY, 2006 (Ph.D. thesis).
[49] K. Brueckner, V. Cimalla, F. Niebelschutz, R. Stephan, K. Tonisch, O. Ambacher, M.A. Hein, Strain- and pressure-dependent RF response of microelectromechanical resonators for sensing applications, Journal of Micromechanics and Microengineering 17 (2007) 2016–2023.